

Source of nonlinearity of the BOLD response revealed by simultaneous fMRI and NIRS

Hiroshi Toyoda,^{a,b} Kenichi Kashikura,^c Tomohisa Okada,^a Satoru Nakashita,^{a,d} Manabu Honda,^a Yoshiharu Yonekura,^e Hideo Kawaguchi,^{b,f} Atsushi Maki,^f and Norihiro Sadato^{a,b,g,*}

^aDepartment of Cerebral Research, National Institute for Physiological Sciences, Okazaki, Japan

^bJST (Japan Science and Technology Corporation)/RISTEX (Research Institute of Science and Technology for Society), Kawaguchi, Japan

^cDepartment of Radiological Technology, Gunma Prefectural College of Health Sciences, Maebashi, Japan

^dDepartment of Physiological Sciences, The Graduate University for Advanced Studies (Sokendai), Kanagawa, Japan

^eBiomedical Imaging Research Center, University of Fukui, Fukui, Japan

^fHitachi, Ltd. Advanced Research Laboratory, Hatoyama, Saitama, Japan

^gDepartment of Functional Neuroimaging, Faculty of Medical Sciences, University of Fukui, Fukui, Japan

Received 5 January 2007; revised 23 August 2007; accepted 27 September 2007

Available online 11 October 2007

The nonlinearity of the blood oxygenation level-dependent (BOLD) response to stimuli of different duration, particularly those of short duration, has been well studied by functional magnetic resonance imaging (fMRI). This nonlinearity is assumed to be due to neural adaptation and the nonlinearity of the response in the oxygen extraction fraction (OEF); the latter has not been examined quantitatively in humans. To evaluate how the OEF response contributes to the nonlinearity of the BOLD response to neural activity, we used simultaneous fMRI and near-infrared spectroscopy (NIRS). The responses to visual stimuli of four different durations were measured as changes in the BOLD signal and the NIRS-derived hemoglobin concentrations. The hemodynamic response nonlinearity was quantified using an impulse response function model with saturation nonlinearity scaling in the response amplitude, assuming that the unknown neural adaptation parameters varied within a physiologically feasible range. Independent of the degree of neural adaptation, the BOLD response consistently showed saturation nonlinearity similar to that of the OEF response estimated from the NIRS measures, the nonlinearity of which was greater than that of the response in the total hemoglobin concentration representing the cerebral blood volume (CBV). We also found that the contribution of the OEF response to the BOLD response was four to seven times greater than the contribution of the CBV response. Thus, we conclude that the nonlinearity of the BOLD response to neural activity originates mainly from that of the OEF response.

© 2007 Elsevier Inc. All rights reserved.

Keywords: BOLD; Deoxyhemoglobin; fMRI; Functional magnetic resonance imaging; Hemodynamic response; Near-infrared spectroscopy; NIRS; Nonlinearity; OEF; Oxygen extraction fraction

Introduction

Functional magnetic resonance imaging (fMRI) detects activation in the brain by measuring changes in the MRI signal during neural stimulation. Blood oxygenation level-dependent (BOLD) fMRI is the most prevalent technique and is sensitive to changes in the concentration of deoxyhemoglobin ([HbR]) in small local blood vessels (Ogawa et al., 1990; Kwong et al., 1992). A decrease in [HbR] follows activation in response to a disproportionately large increase in cerebral blood flow (CBF) accompanying a smaller increase in the cerebral metabolic rate of oxygen (CMRO₂; Fox and Raichle, 1986; Fox et al., 1988). However, the details of these dynamics are complex (for a review, see Buxton et al., 2004).

To accurately interpret the functional data, it is critical to understand the relationships between the stimulus parameters and the hemodynamic response. Boynton et al. (1996) suggested a linear relationship between stimulus duration and the BOLD signal response. However, recent studies have shown nonlinearity of the BOLD response to stimulus parameters such as duration, rate, and amplitude (Soltysik et al., 2004, and references therein). Stimuli with shorter durations produce larger signal increases than expected from a linear system (Vazquez and Noll, 1998; Birn et al., 2001; Pfeuffer et al., 2003; Soltysik et al., 2004). In the primary visual cortex, the threshold between linear and nonlinear ranges was reported to have a stimulus duration of 3 to 4 s (Vazquez and Noll, 1998; Liu et al., 2000; Soltysik et al., 2004). Whether the BOLD response to a stimulus is linear or nonlinear with respect to the stimulus parameters is an important consideration in the design and analysis of fMRI studies, especially in event-related designs. A nonlinear relationship might cause the estimates of the BOLD change at longer stimulus

* Corresponding author. Section of Cerebral Integration, Department of Cerebral Research, National Institute for Physiological Sciences, Myodaiji, Okazaki, Aichi, 444-8585, Japan. Fax: +81 564 55 7786.

E-mail address: sadato@nips.ac.jp (N. Sadato).

Available online on ScienceDirect (www.sciencedirect.com).

durations to be overpredicted using linear extrapolation of the response at shorter stimulus durations.

The current hemodynamic models include the following potential candidates for the origin of the nonlinearity of the BOLD response: first, the neuronal response (activation/inhibition) to stimuli; second, the coupling of the regional blood flow to the neuronal response; third, the relationship between blood flow and volume (Grubb et al., 1974); and fourth, the relationship between blood flow and the oxygen extraction fraction or OEF (Buxton and Frank, 1997; Buxton et al., 1998; Friston et al., 2000). Due to the experimental set-up used in the present study, only the CBV, [HbR], and OEF were investigated while examining the influence of the nonlinearity of neuronal activity.

Neural adaptation has been proposed as a possible source of the BOLD nonlinearities in the visual cortex (Boynton et al., 1996; Logothetis et al., 2001) and the auditory cortex (Robson et al., 1998). This hypothesis is supported by a research that demonstrated a greater BOLD response to stimuli with shorter durations than would be predicted from the response to stimuli with longer durations using linear system analysis (Miller et al., 2001). Logothetis et al. (2001) measured the BOLD response associated with the field potential in the monkey V1 cortex. In addition, a multimodal study using the BOLD approach and electroencephalography in humans (Janz et al., 2001) demonstrated the adaptation phenomenon in the electroencephalogram amplitude; however, this research also suggested that neural adaptation alone could not explain the nonlinearity of the BOLD response to the stimuli.

Another possible source of the nonlinearity observed in the BOLD response to neural stimuli is the OEF response. Several studies, including that of Miller et al. (2001), have suggested that there is a nonlinear transformation from the CBF response to the BOLD response. An early study using positron emission tomography (PET) and fMRI (Rees et al., 1997) also indicated that nonlinearity occurred in the transformation of neural activity into the BOLD response. In this case, the PET-measured CBF response was linear, while the BOLD response was nonlinear. The authors proposed that this discrepancy was caused by the nonlinear OEF response. The saturation nonlinearity of the OEF response is attributed to nonlinear coupling between the CBF and oxygen metabolism (Buxton and Frank, 1997). Although the nonlinear OEF response has been clearly established theoretically, there is little quantitative evidence of this phenomenon or its contribution to the nonlinearity of the BOLD response, especially in humans.

The relationships among the CBF, OEF, and BOLD contrast during neural activation have been demonstrated directly by both PET and fMRI measurements in human subjects. A recent PET and fMRI study showed a significant positive correlation between changes in the CBF and the BOLD signal, and a significant negative correlation between changes in the OEF and the BOLD signal (Ito et al., 2005). This finding implies that the CBF and OEF are negatively correlated. However, the level of nonlinearity cannot be estimated sensitively from correlation analysis alone. To accurately quantify the level of the response nonlinearity, it would be preferable to use an analysis with an impulse response function (IRF) model (Boynton et al., 1996; Soltysik et al., 2004). IRF models cannot be applied to PET because of the poor temporal resolution.

Recent advances in near-infrared spectroscopy (NIRS) have facilitated the accurate and noninvasive measurement of the time course of the oxyhemoglobin concentration ([HbO]) and [HbR] during neural activation in humans (Villringer et al., 1993, 1994). It

is also possible to use NIRS in combination with electroencephalography to demonstrate neurovascular coupling (Obrig et al., 2002). The greatest merit of this optical imaging technique lies in the fact that the hemoglobin concentration can be separately monitored with high temporal resolution. In contrast to PET, NIRS measurements can be performed simultaneously with fMRI and can elucidate the temporal dynamics of the responses during and after the stimulus. The simultaneous measurement of fMRI and NIRS can provide data from both measures which are time-locked responses to the same stimuli. Thus, the linearity/nonlinearity of these responses can be estimated under identical conditions. Several reports of the simultaneous measurement of fMRI and NIRS have previously been published (Kleinschmidt et al., 1996; Punwani et al., 1998; Toronov et al., 2001; Mehagnoul-Schipper et al., 2002; Strangman et al., 2002; MacIntosh et al., 2003; Huppert et al., 2006). These studies provide convincing evidence for the correlation between the two methodologies.

Wobst et al. (2001) previously investigated the [HbR] responses to various visual durations in the linear range (that is, longer than 3–4 s). They showed that the [HbR] response was linear with respect to visual stimuli with durations of 3–24 s. However, in the nonlinear range of stimulus duration (that is, shorter than 3–4 s), NIRS has not yet been utilized to investigate the nonlinearity of the BOLD response with respect to the stimulus duration.

The purpose of the present study was to investigate the origin of the nonlinearity of the BOLD signal response with respect to stimulus duration, using the simultaneous measurement of fMRI and NIRS. NIRS-measured responses were compared with the BOLD response in terms of their nonlinearity. The responses of the OEF and CBV were estimated from the NIRS measurements and were compared with the BOLD response. To quantify the level of nonlinearity of these responses, we proposed an IRF model with saturation nonlinearity scaling in the response amplitude. The model could explicitly include the nonlinear neural response to stimulus (neural adaptation). In the present analysis, the unknown neural adaptation was assumed to vary within the physiologically feasible range, and the degree of nonlinearity of the responses to the assumed neural activity was estimated for each level of neural adaptation. In addition, the model proposed by Obata et al. (2004) was applied to the simultaneously measured fMRI and NIRS data (Huppert et al., 2006). This allowed quantitative evaluation of the contribution of the OEF and CBV to the BOLD signal. Our hypothesis was that the nonlinearity of the BOLD response to neural activation was mainly due to the nonlinearity of the OEF response.

Materials and methods

Subjects

Five healthy volunteers (one male and four female; age range=20–29 years) participated in this study. All subjects had normal or corrected-to-normal visual acuity. The protocol was approved by the ethical committee of Fukui University School of Medicine, Japan, and all subjects gave their written informed consent for participation in the study.

Task presentation

Each subject lay supine in an MRI scanner containing NIRS optodes and observed the stimuli in a mirror that was mounted on

the head coil directly above their eyes. The visual stimulus was a black-and-white circular checkerboard pattern with a central fixation cross, which reversed at a frequency of 8 Hz and was projected onto a ground-glass screen at a visual angle of $\sim 10^\circ$ from the subject's eyes. For each subject, 10 sessions were carried out in total. Each session consisted of four stimuli of different duration (1, 2, 4, and 8 s) presented in a random order with a fixed interval of 20 s. Each stimulus duration was presented once per session. The visual stimulus during rest periods was a small fixation cross positioned at the center of the circular checkerboard pattern. The subjects were instructed to maintain stable binocular fixation on the cross during both the rest and task periods. The timing of the task presentations was synchronized with the fMRI scan by trigger pulses from the system.

fMRI measurements

A time series of 102 volumes was acquired for each session using T2*-weighted gradient-echo echo-planar imaging (EPI) sequences using a 3-T MR imager (GE Medical Systems, Milwaukee, WI, USA). Each volume consisted of five slices, each of which was 4.0 mm thick, with a 1.0-mm gap, in order to cover the entire primary visual cortex. The time interval between two successive acquisitions of the same slice (TR) was 1035 ms with a flip angle (FA) of 70° and an echo time (TE) of 30 ms. The field of view (FOV) was 220 mm and the in-plane matrix size was 64×64 pixels. The session was repeated 10 times. For anatomical reference, T2-weighted fast spin-echo images (TR=4000 ms; TE=68 ms; FA= 90° ; FOV=220 mm; matrix size= 256×256 mm) were collected at the same positions as the echo-planar images. The same sequence was utilized to cover the entire brain with higher spatial resolution (slice thickness=1.5 mm; a total of 92 transaxial images).

Optode location identification and NIRS signal-source estimation

T2-weighted whole-brain anatomical MR images were resliced and interpolated into an image with an iso-voxel size of $1 \times 1 \times 1$ mm. The optode locations were then identified from the dimples of the scalp surface on the anatomical MR images (Fig. 1). The channel with the largest response was selected to be used in the subsequent analysis. On the basis of Maki et al. (1995), the NIRS signal source was assumed to be localized in the spherical area (diameter=15 mm) located 20 mm below the mid-point of the paired optodes (Fig. 1). T2-weighted whole-brain anatomical MRI data were coregistered into T2-weighted coplanar anatomical MRI data using imaging header information, so as to match the coordinate system. Using this coordinate matching, the optode positions on the T2-weighted whole-brain anatomical MR images could be transformed into a T2-weighted coplanar anatomical MRI coordinate system, resulting in coregistration of the estimated NIRS signal-source regions of interest (ROIs) into T2-weighted coplanar anatomical MRI data.

Every fMRI slice for each time-point was realigned into the corresponding slice of the T2-weighted coplanar anatomical MRI data by an in-house program written in the C language using a non-rigid transformation algorithm (Ardekani et al., 1995, 2005). The coregistration was performed by a rigid body transform and a nonlinear transform, the latter of which allowed local unwarping to correct the distorted EPI. The head motion and

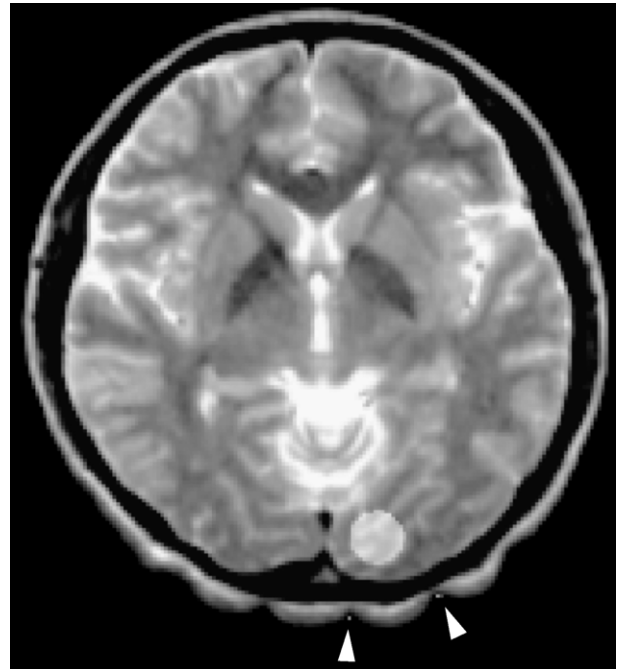


Fig. 1. Location of the optodes and NIRS signal-source estimation in anatomical MRI. Representative image showing the tips of a pair of optodes identified at the dimpled surface of the scalp (arrowheads). In this anatomical MR image, the shaded circular region represents the NIRS signal source. This was estimated as a spherical-shaped ROI (diameter=15 mm), the center of which was assumed to be set at a 20-mm depth from the scalp surface midway between the paired optodes.

distortion corrections for the EPI were incorporated into this process. We visually confirmed that there was good matching of the brain surfaces between the anatomical MRI and realigned fMRI data using this process. The ROI for the estimated NIRS signal source on the MRI data was also used for the corresponding fMRI time series data. The fMRI time series data from the ROI were time locked to the stimulus onset (stimulus locked) and extracted for each of the durations. The segmented stimulus-locked fMRI time series data were corrected for baseline drift in the same manner as described for NIRS signal processing. For each subject, stimulus-locked averaging was performed across all repeated sessions. This resulted in an fMRI response curve for each of the durations.

NIRS measurements

Optical data recordings were made using a multi-channel NIRS instrument (ETG-100, Hitachi Medical Corporation, Japan). Two wavelengths of NIR light (780 and 830 nm) were generated by the instrument equipped with 20 laser diodes (10 per wavelength) and detected by eight avalanche photo-diodes. The frequency for the sampling absorbance was 10 Hz. The light in all channels was guided separately towards and away from the instrument by optical fibers (diameter=1 mm; length=10 m). The optical fibers and optodes were constructed from anti-magnetic materials to allow simultaneous measurements with MRI. The optodes were positioned over the occipital region of each subject's

head. Using an optode holder, the inter-optode distance was set to be ~3 cm, although it varied due to local differences in head shape. A single measurement channel was configured with a pair of incident and detection optodes, allowing changes in absorbance for both wavelengths to be measured simultaneously. The absorbance data for each channel were recorded continuously onto the hard disk of the NIRS instrument throughout the fMRI scanning sessions.

NIRS analysis

The response data for each of the durations were stimulus locked and extracted from the raw absorbance measurements, which were continuously sampled for each channel. To remove the pulsatile fluctuation from the task-related physiological response, a moving average was taken over 20 observation points (2 s) from the absorbance time series data. The baseline drift in the absorbance data was then corrected by linear interpolation between the pre-change and post-change periods. This operation was intended to adjust the levels between the values at the stimulus onset and the response end so as to flatten them. The changes in absorbance for both 780 and 830 nm wavelengths were stimulus locked and averaged across all 10 sessions for each of the durations. Finally, the corrected absorbance data were converted to relative changes in [HbO] and [HbR] using the modified Beer–Lambert (MBL) law (Cope and Delpy, 1988; Chance, 1991; Villringer and Chance, 1997). The MBL equation requires an assumption about the differential path-length factor (DPF); here, we assumed that the DPF=6 for both wavelengths (Duncan et al., 1995). The relative change in [HbT] was calculated as a sum of the changes in [HbO] and [HbR]. A single recording channel that responded maximally to the stimuli was selected for each subject. The individually calculated response data were then averaged across all subjects for each stimulus duration.

OEF estimation from NIRS measurements

The OEF response can be approximated from the NIRS-measured [HbR] and [HbT] responses. The OEF (E) can be defined based on the arterial and venous blood oxygenation levels (Y_a and Y_v , respectively; van Zijl et al., 1998; Oja et al., 1999) according to Eq. (1).

$$E = 1 - Y_v/Y_a \quad (1)$$

The total blood oxygenation (Y_t) can be formulated using a compartmental model as shown in Eq. (2), as the optical signals originating from the hemoglobin in the tissue should be a mixture of arterial and venous blood (Culver et al., 2003).

$$Y_t = (1 - \gamma)Y_a + \gamma Y_v \quad (2)$$

Here, γ represents the venous blood volume fraction (that is, the venous blood volume divided by the total blood volume or $\gamma \equiv V_v / V_t$).

With NIRS measurements, Y_t can be given by Eq. (3).

$$Y_t = \frac{[\text{HbO}]}{[\text{HbT}]} = 1 - \frac{[\text{HbR}]}{[\text{HbT}]} \quad (3)$$

From Eqs. (1)–(3), assuming Y_a to be unity and γ to be constant during activation (Culver et al., 2003), the baseline normalized OEF ($E(t)/E(0) \equiv e$) can be described with the baseline normalized [HbR] and [HbT] as shown in Eq. (4).

$$e \equiv \frac{E(t)}{E(0)} \approx \frac{[\text{HbR}]/[\text{HbR}]_0}{[\text{HbT}]/[\text{HbT}]_0} \quad (4)$$

IRF model and response nonlinearity

In the present study, we used an IRF model to estimate the nonlinearity of the responses in the BOLD signal and the NIRS-measured hemoglobin concentration (Boynton et al., 1996; Pfeuffer et al., 2003; Soltysik et al., 2004). Our model is illustrated in Fig. 2. The transformation of the stimulus into the BOLD signal response can be separated into two steps: first, the step from the stimulus to the neural response; and second, the step from the neural response to the BOLD signal response.

We assumed that the nonlinearity in the first step was simply modeled with a neural adaptation function as shown in Eq. (5).

$$n(t) = s(t) \cdot \{a \cdot \exp(-t/b) + 1\} \quad (5)$$

Here, t is the time after stimulus onset, $n(t)$ and $s(t)$ represent the neural response function and stimulus function, respectively, and a and b represent the parameters characterizing the neural adaptation function (Miller et al., 2001; Soltysik et al., 2004). Parameter a is the initial offset for the level of neuronal activity and parameter b is the decay constant.

The $n(t)$ was convolved with an IRF ($h(t)$) to produce the estimated responses of the BOLD signal and hemoglobin concentration. In this study, the $h(t)$ was modeled using a gamma-variate function (Boynton et al., 1996; Soltysik et al., 2004) as described in Eq. (6).

$$h(t) = \alpha \cdot \left(\frac{t}{\tau}\right)^\beta \cdot \exp\left(-\frac{t}{\tau}\right) \quad (6)$$

Here, α , β , and τ are free parameters characterizing $h(t)$. By definition, if the $h(t)$ function is estimated to be identical for different $n(t)$ functions, the response in the BOLD or hemoglobin concentration is linear to $n(t)$. By contrast, if the $h(t)$ function is estimated to vary for different $n(t)$ functions, the response to $n(t)$ is nonlinear. Thus, in the present study, we estimated the $h(t)$ for four different stimulus durations in the BOLD and hemoglobin concentration responses, in order to assess the response nonlinearity in terms of the stimulus duration.

Furthermore, to quantify the nonlinearity in the second step, we introduced the nonlinear scaling transformation shown in Eq. (7), which was described by a saturation curve as a function of the stimulus duration. The $n(t)$ convolved with $h(t)$ was scaled by a factor written as (D^ρ/D), where D was the stimulus duration, and the exponent ρ was a free parameter characterizing the degree of saturation nonlinearity (in this study, ρ was therefore defined as the saturation nonlinearity index or SNI).

$$r(t) = n(t) \otimes h(t) \cdot \frac{D^\rho}{D} \quad (7)$$

Based on the model described in Eqs. (5) and (7), the measured responses in the BOLD signal and hemoglobin concentration were fitted using a least squares method. The free parameters for the

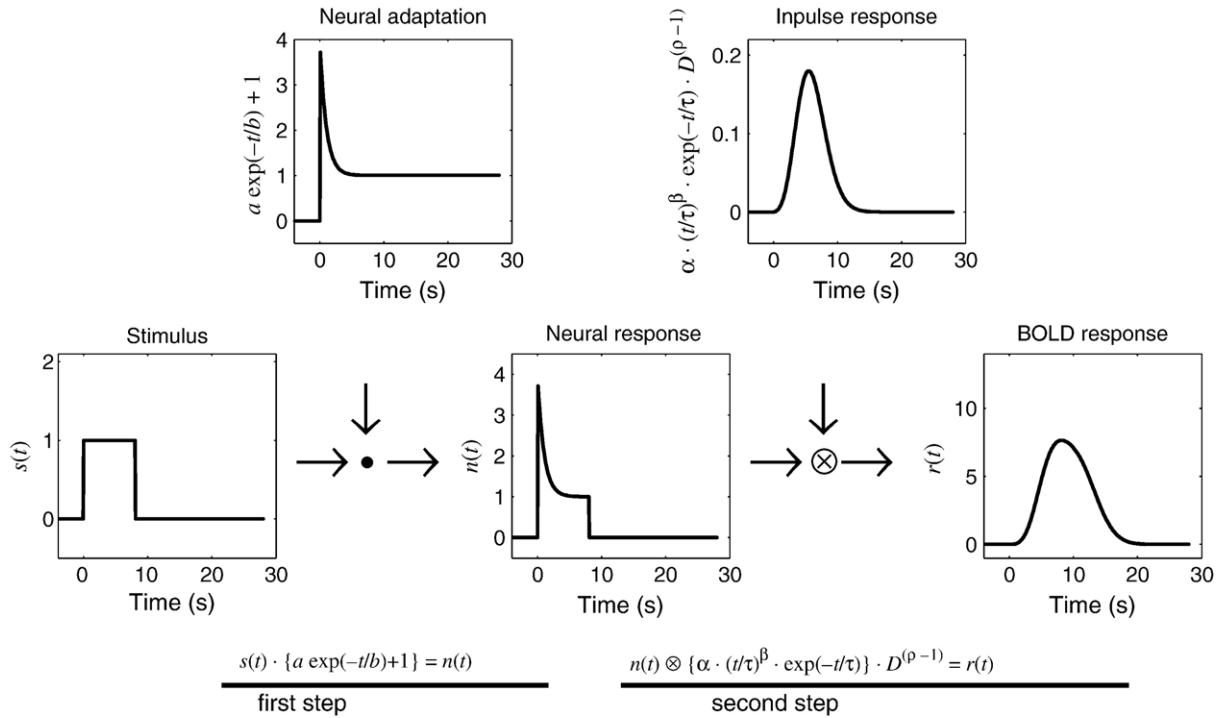


Fig. 2. Nonlinear transform model for the transition from the stimulus to the BOLD signal response. An $s(t)$ with a constant amplitude, multiplied by the neural adaptation function, modeled as a function in which an initial strong response decays to a lower steady-state value (Eq. (5)), yields $n(t)$. The latter can be convolved with an IRF, $h(t)$ (Eq. (6)) and multiplied by a scaling factor (D^ρ/D) to yield the estimated BOLD response function ($r(t)$) (Eq. (7)), where D represents the stimulus duration and the exponent ρ of the power function denotes the saturation nonlinearity index characterizing the degree of nonlinearity in the second step.

model (α , β , τ , and ρ) in Eqs. (6) and (7) were estimated using a best-fit model. If the fitted value of ρ was equal to unity, the scaling process was an identical transformation, indicating that the response $r(t)$ was linear to $n(t)$. A ρ value of less than unity indicated a larger degree of saturation nonlinearity with increasing stimulus duration.

Simulation of various neural adaptation functions

Simulations were performed to assess the effect of the neural adaptation function described in Eq. (5), as the neural response was not measured in the present study. As described above, we used a model (Fig. 2) that included neural adaptation. However, in our analysis, the neural adaptation parameters (a and b in Eq. (5)) were not determined from experimental data, as it was difficult to estimate the nonlinearity parameters for both the first and second steps simultaneously using a least-squares fitting technique. Instead, the unknown neural adaptation in the first step (Fig. 2) was varied within the physiologically feasible range: $0 \leq a \leq 3$ in increments of 0.5 and $0.1 \leq b \leq 0.9$ in increments of 0.1 in Eq. (5) (Miller et al., 2001; Soltysik et al., 2004). This simulation approach allowed us to evaluate how variation affected the estimation of the response nonlinearity in the second step.

Simulation of assumed parameters

Simulations were carried out to examine the feasibility of the other assumed variables in the present analysis (that is, the baseline values for [HbT], and Y_t). These unknown parameters

were assumed to match the values reported in the literature. This could have introduced errors into the results of the estimations. In the simulations, the SNI was estimated for [HbT]₀ values ranging from 40 to 200 μM , and for $Y_t(0)$ values ranging from 60 to 80%.

BOLD model

Independent of the aforementioned nonlinearity analysis, we investigated the components of the BOLD signal response by applying the model proposed by Obata et al. (2004) to our simultaneously measured fMRI and NIRS data. The model explicitly deals with the variables of the balloon model, which was originally proposed by Buxton et al. (1998). The derivation of this model was based on separate estimates of the intravascular and extravascular signal changes (Buxton et al., 1998, 2004). As the variables of the balloon model can be approximately related to [HbR] and [HbT], the model has been applied to compare fMRI data with optical intrinsic imaging or NIRS findings (Hess et al., 2000; Huppert et al., 2006). Although the balloon model was derived theoretically, it has been refined and tested with experimental data (Feng et al., 2001; Friston, 2002; Mildner et al., 2001; Toronov et al., 2003; Obata et al., 2004). The model has also been tested with response data obtained from fMRI and optical recording or NIRS (Hess et al., 2000; Huppert et al., 2006), which have verified the model.

Using the model, the fractional change in BOLD signal ($S(t)$) can be expressed as a linear sum of the changes in the baseline-normalized deoxyhemoglobin content per volume (q) and the

baseline-normalized venous blood volume fraction (v) as shown in Eq. (8).

$$\Delta S(t)/S(0) = A \cdot (1 - q) + B \cdot (v - 1) \equiv f(q, v) \quad (8)$$

Here, A and B are constant parameters that depend on several experimental and physiological parameters.

This model can be tested with simultaneously measured NIRS and fMRI data, as q and v can be approximated using the baseline-normalized [HbR] and [HbT] values, respectively, as measured by NIRS (Strangman et al., 2002; Huppert et al., 2006). By definition, the baseline-normalized deoxyhemoglobin content per unit volume (q) is equivalent to the baseline-normalized [HbR], as described in Eq. (9).

$$q \equiv \frac{[\text{HbR}]}{[\text{HbR}]_0} \quad (9)$$

The baseline-normalized venous blood volume ($V_v(t)/V_v(0) \equiv v$) can be assumed to be equal to the baseline-normalized total blood volume ($V_t(t)/V_t(0)$) when the venous blood volume fraction ($V_v(t)/V_t(t) \equiv \gamma(t)$) is constant during activation (Culver et al., 2003). In addition, the baseline-normalized V_t can be assumed to be equal to the baseline-normalized [HbT] if the hematocrit (Hct) level is constant during activation (Boas et al., 2003, but see Kleinfeld et al., 1998; Vanzetta et al., 2005), as shown in Eq. (10).

$$v \equiv \frac{V_v(t)}{V_v(0)} \approx \frac{V_t(t)}{V_t(0)} \approx \frac{[\text{HbT}]}{[\text{HbT}]_0} \quad (10)$$

In the present analysis, the model shown in Eq. (8) was tested with our measured fMRI and NIRS data using a least-squares fitting technique to estimate the constant parameters A and B . For the least-squares fitting, we used the standard built-in function ‘fminsearch’ implemented in Matlab (Version 7). As this method is suitable for local optimization, the fitting results might be influenced by the initial values of the parameter estimates. To exclude this possibility, we adopted a multi-start local optimization approach using this method. Based on the estimated A and B values, the mixture ratio between q and v in the total BOLD signal change was determined as a ratio of the coefficients in Eq. (8) (that is, A/B ; Huppert et al., 2006).

Contribution ratio of OEF and CBV to BOLD

To evaluate the q and v contributions to the BOLD response, the q and v responses were plotted as a trajectory in the q - v plane with the contours of the BOLD signal changes estimated from Eq. (8) (Buxton et al., 2004). The plot in the q - v plane depicts the relationship of the change in q and v to the BOLD signal change $f(q, v)$. The slope of the equal-BOLD contour, which is constant in the q - v plane, represents the mixture ratio, A/B , indicating that the fractional change of q brings an A/B times larger change in the BOLD signal than that of v . The constant slope of the straight contour indicates that the contributions of q and v to $f(q, v)$ are $f(q, 1)$ and $f(1, q)$, respectively, and the sum of these contributions is identical to $f(q, v)$. These can be confirmed graphically in the q - v plane. Thus, the contribution ratio at the peak of the BOLD response is defined as $A(1 - q_p)/B(v_p - 1) = f(q_p, 1)/f(1, v_p)$, given that the peak BOLD response occurs at $q = q_p$ and $v = v_p$.

Furthermore, in analogy with the plot in the q - v plane, we attempted to plot the baseline normalized OEF response (e) with

the v response as a trajectory in the e - v plane to evaluate the e and v contributions to the BOLD response. q could be expressed simply as the product of e and v (Eqs. (9) and (10)) as follows:

$$q \approx e \cdot v \quad (11)$$

Thus, Eq. (8) was transformed into a formula that described the BOLD signal change as a function of the e and v responses, instead of the q and v responses:

$$\Delta S(t)/S(0) \approx A \cdot (1 - e \cdot v) + B \cdot (v - 1) \equiv g(e, v) \quad (12)$$

In this case, $g(e, v)$ could not be expressed as a linear sum of the contributions of e and v . However, the contributions of the e and v components to $g(e, v)$ were graphically approximated as $g(e, 1)$ and $g(1, v)$, respectively, using the plot in the e - v plane, because the contour line was found to be almost straight and constant within the physiological range of e and v changes. For this reason, we estimated the contribution ratio as $|g(e_p, 1)/g(1, v_p)|$, given that the peak BOLD response occurs at $e = e_p$ and $v = v_p$.

Results

Stimulus-locked time courses of measured NIRS and fMRI responses

The plots of the averaged time courses of the stimulus-locked responses in NIRS and fMRI are shown in Fig. 3. There was a task-related increase in [HbO] and a smaller decrease in [HbR], yielding an increase in [HbT]. For all of the measures, the absolute peak amplitude increased monotonically with increasing stimulus duration. However, the peak amplitude ratio between the $\Delta[\text{HbR}]$ and $\Delta[\text{HbT}]$ responses was not constant with respect to stimulus duration: the peak amplitude ratio between $\Delta[\text{HbR}]:\Delta[\text{HbT}]$ was about 1:2 for a stimulus duration of 8 s, compared with 1:1 for a stimulus duration of 2 s (Fig. 3).

Correlation analysis between NIRS and fMRI measurements

The similarities of the response waveforms among the measures were evaluated by correlation analysis. For stimulus durations of 1, 2, 4, and 8 s, the Pearson's correlation coefficients of the averaged responses between BOLD and [HbR] were 0.963, 0.976, 0.990, and 0.993, respectively, while those between BOLD and [HbT] were 0.910, 0.939, 0.974, and 0.983, respectively. All of the correlations were highly statistically significant ($p < 10^{-4}$). For each of the stimulus durations, the BOLD response showed a slightly greater correlation with the [HbR] response than with the other NIRS-measured hemoglobin concentration.

Nonlinearity estimation with the proposed IRF model

As shown in Fig. 4, the estimated OEF response, as well as the measured [HbT], [HbR], and BOLD responses, were fitted by the proposed IRF model (Fig. 2). Given the greater neural adaptation – that is, the greater value for a or b in Eq. (5) – a larger SNI index for the response nonlinearity in the second step was expected for the measured and estimated responses (Table 1). Thus, the SNI was estimated to be an increasing function of the neural adaptation parameters (Fig. 5). By contrast, regardless of the degree of neural adaptation, the shape of the normalized IRF was similar for each of the measured and estimated responses. The measured and

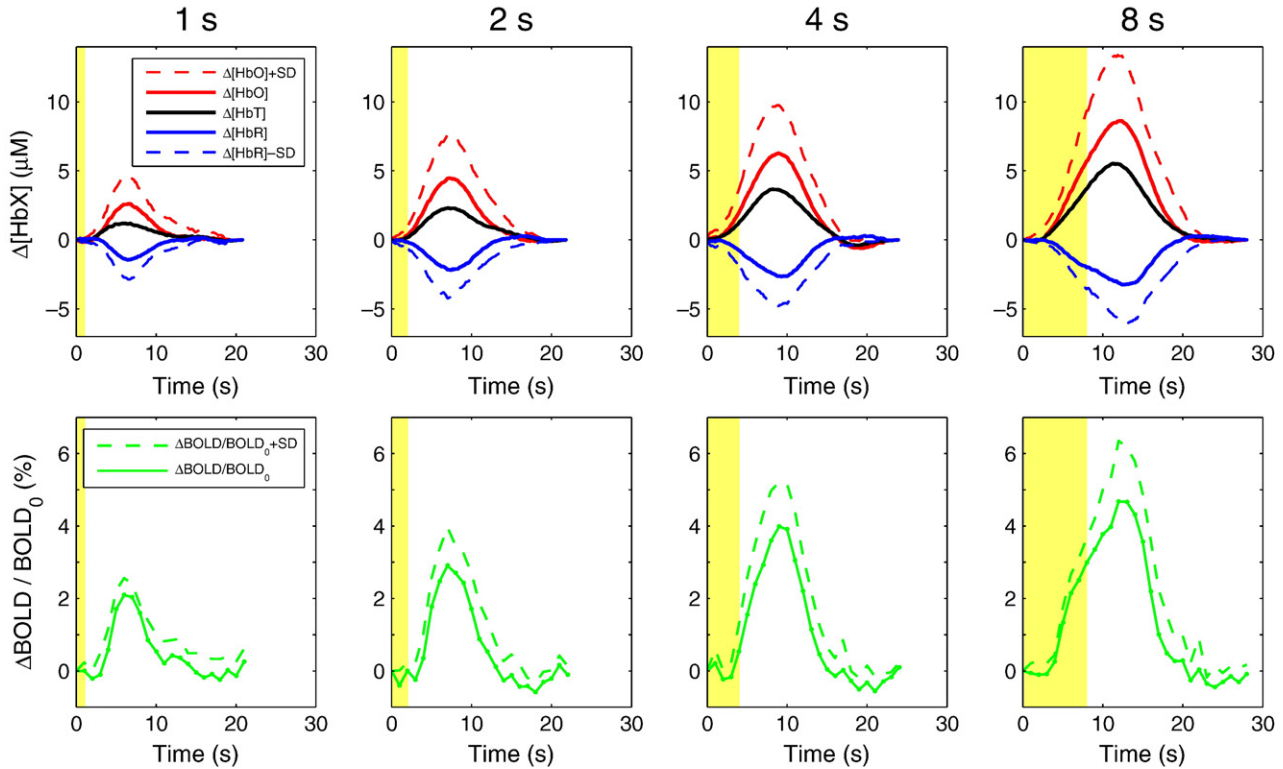


Fig. 3. Plots of the averaged time course of the measured responses in NIRS (top) and fMRI (bottom; stimulus-locked average across all subjects; $n=5$). In order to remove the pulsatile fluctuation in the original absorption curves, a 20-point (2-s) moving average was applied to the curves. Shaded areas indicate stimulus presentation times. The response curves for the same stimulus duration are similar in shape but have different amplitudes, except for the [HbR] response. In all measures, the absolute value of the peak amplitudes increases monotonically with increasing stimulus duration.

estimated [HbT], [HbO], [HbR], and BOLD responses to the neural response showed varying degrees of nonlinearity with respect to the stimulus duration.

Regardless of the degree of unknown neural adaptation, the SNI of the [HbT] response was the largest while that of the [HbR] response was relatively small. This apparent difference in the nonlinearity between the responses was attributed to the nonlinear nature of the OEF response (see the Materials and methods section). The SNI of the estimated OEF response was less than that of the [HbT] response. Regardless of the degree of neural adaptation, the nonlinearity of the OEF response was similar to that of the BOLD responses (Fig. 5), even though they were derived separately. These results suggest that the OEF might be the main origin of the nonlinearity of the BOLD responses.

Contribution of q - v ratio to BOLD signal change

Assuming that the mixture ratio between q and v (the A/B ratio) is constant for all of the stimulus durations, the BOLD response estimated using the model of Eq. (8) consistently fitted the measured response (Fig. 6). The A/B ratio was estimated to be 4.68:1, assuming that the baseline value for [HbT] was 85 μM , the baseline value for the venous blood oxygenation level ($Y_v(0)$) was 0.65, the venous blood volume fraction γ was 0.75, and the baseline value for the total blood volume fraction $V_t(0)$ was 0.04.

The peak amplitude of the $(1-q)$ response was greater than that of the $(v-1)$ response for all of the stimulus durations (Fig. 6A). However, the peak ratio between $(1-q)$ and $(v-1)$ decreased as the

stimulus duration increased, suggesting a difference in the nonlinearity between the two responses. As an A/B of 4.68 should enhance the peak ratio between $(1-q)$ and $(v-1)$, the contribution ratio between $A \cdot (1-q)$ and $B \cdot (v-1)$ was estimated in terms of the model of Eq. (8) to be 10–22:1 (Fig. 6B). This indicated that the BOLD response mostly consisted of the q response, which was at least 10 times more influential than the v response.

Plots in the q - v and e - v planes

According to the trajectory plots in the q - v plane (Fig. 7A), the decrease in q contributed greatly to the BOLD signal increase, whereas the increase in v contributed relatively little. The contribution ratio between q and v at the peak BOLD change ($f(q=q_p, v=v_p)$), as graphically estimated by $f(q_p, 1)/f(1, v_p)$, was 20.2 ($=1.82/0.09$) for 1-s duration, 16.5 ($=2.81/0.17$) for 2-s duration, 13.2 ($=3.43/0.26$) for 4-s duration, and 10.8 ($=4.23/0.39$) for 8-s duration (Fig. 7A). As the stimulus duration increased, the contribution ratio decreased in association with the decrease in the peak amplitude ratio (Fig. 7A).

Similarly, the e and v contributions at the peak BOLD change ($g(e=e_p, v=v_p)$), were estimated graphically by $g(e_p, 1)$ and $g(1, v_p)$, respectively, the values of which were 2.19 and 0.31% for the duration of 1 s, 3.50 and -0.62% for the duration of 2 s, 4.45 and -0.94% , for the duration of 4 s, and 5.70 and -1.44% for the duration of 8 s. The negative value of $g(1, v_p)$ suggested that the effect of the v response, given the constant e , was negative with respect to the BOLD signal increase. The e and v contribution ratio,

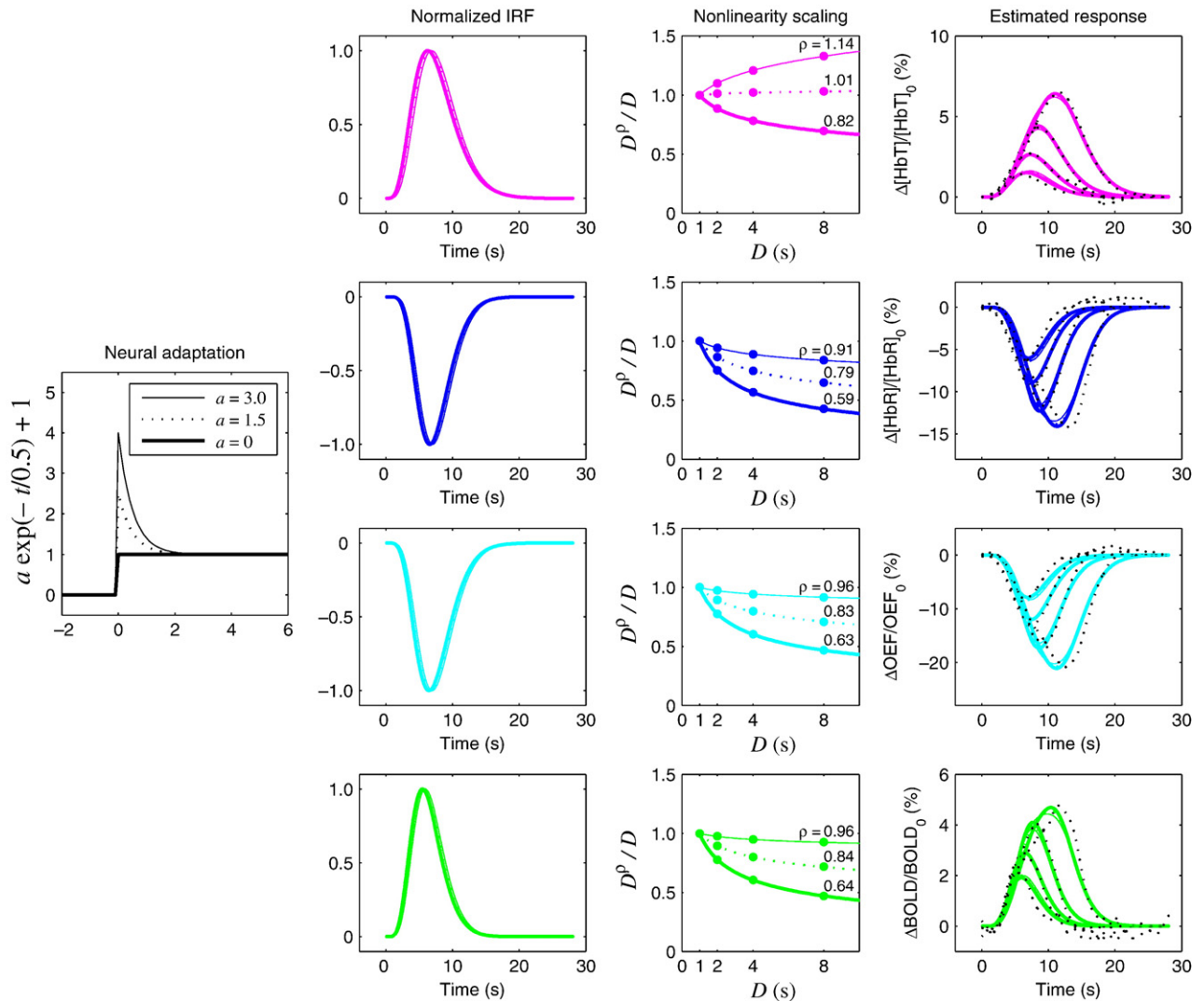


Fig. 4. Results of the application of the proposed model (Fig. 2) to the responses in [HbT] (top row), [HbR] (second row), OEF (third row), and BOLD (bottom row). For each response, the IRF and SNI were estimated by curve fitting, under the assumption of various strengths of neural adaptation. Representative cases are shown here with parameters of $a=0, 1.5, 3.0$, and $b=0.5$ for the neural adaptation function (Eq. (5)). The estimated SNI value differs between these responses, suggesting differences in the degrees of nonlinearity of the responses in the second step. Regardless of the degree of neural adaptation, the SNI of the [HbT] response was consistently greater than that of any other response. In all of the responses, increasing the neural adaptation parameter a increased the SNI, whereas the shape of the IRF remained relatively unchanged.

as estimated by $|g(e_p, 1)/g(1, v_p)|$, was 7.1 ($=2.19/0.31$) for the duration of 1 s, 5.6 ($=3.50/0.62$) for the duration of 2 s, 4.7 ($=4.45/0.94$) for the duration of 4 s, and 4.0 ($=5.70/1.44$) for the duration of 8 s. This indicated that the OEF decrease contributed greatly to the BOLD signal increase, while the CBV contributed relatively little to the BOLD signal change.

Error in SNI estimates of OEF response caused by estimated variables

The SNI estimation of the OEF response was not sensitive to variation in the assumed baseline values of [HbT] and Y_v , which were selected to fall within the physiologically feasible range (Fig. 8A). The percentage errors in the estimates of SNI were plotted as a function of the errors in the assumed baseline variables (Figs. 8B, C). The plots indicated that the errors in the

SNI estimates of the OEF response were negligible compared with those in the assumed baseline variables, although the results were slightly affected by these errors.

Error in estimates associated with the model of Eq. (8) caused by assumed variables

The estimates of the A/B ratio were sensitive to the assumed baseline value of $Y_v(0)$, which particularly affected the estimates of parameter A . When $Y_v(0)$ varied within the physiologically feasible range from 0.56 to 0.74, $Y_v(0)$ varied from 0.67 to 0.80 (-9 to $+9\%$), A varied from 0.365 to 0.216 ($+26$ to -26%), and A/B varied from 5.88 to 3.48 ($+26$ to -26%). B was unchanged. Hence, the e and v contribution ratio was sensitive to variations in $Y_v(0)$ within the same range, whereas the q and v contribution ratio was insensitive to these changes. However, even if the assumed value

Table 1
The estimated SNI and IRF parameters for various assumptions of neural adaptation

a	0	1	2	3	4	2	2	2	2	2
b	0.5	0.5	0.5	0.5	0.5	0.1	0.3	0.5	0.7	0.9
<i>(i) SNI</i>										
[HbT]	0.82	0.96	1.06	1.14	1.20	0.92	1.00	1.06	1.10	1.12
[HbO]	0.73	0.87	0.97	1.05	1.11	0.83	0.91	0.97	1.00	1.02
[HbR]	0.59	0.73	0.84	0.91	0.97	0.69	0.78	0.84	0.87	0.88
OEF	0.63	0.78	0.88	0.96	1.02	0.73	0.82	0.88	0.91	0.93
fMRI	0.64	0.78	0.89	0.96	1.02	0.74	0.83	0.89	0.92	0.93
<i>(ii) t_{max} (s)</i>										
[HbT]	6.24	6.48	6.67	6.83	6.98	6.41	6.56	6.67	6.74	6.79
[HbO]	6.38	6.59	6.76	6.91	7.03	6.54	6.68	6.76	6.82	6.85
[HbR]	6.55	6.73	6.87	6.98	7.07	6.70	6.81	6.87	6.90	6.92
OEF	6.45	6.64	6.79	6.92	7.02	6.60	6.72	6.79	6.84	6.86
fMRI	6.56	6.73	6.87	6.98	7.08	6.70	6.81	6.87	6.91	6.93
<i>(iii) FWHM (s)</i>										
[HbT]	6.96	6.91	6.92	6.95	7.01	6.89	6.88	6.92	6.98	7.04
[HbO]	6.45	6.40	6.41	6.46	6.54	6.36	6.36	6.41	6.49	6.56
[HbR]	5.71	5.67	5.70	5.77	5.86	5.62	5.63	5.70	5.79	5.87
OEF	6.13	6.08	6.10	6.16	6.24	6.04	6.04	6.10	6.18	6.26
fMRI	5.28	5.25	5.29	5.37	5.47	5.19	5.20	5.29	5.38	5.47

a and b represent the parameters characterizing neural adaptation function (Eq. (5)).

for $Y_v(0)$ differed from the actual value, as long as it varied within the range described above, the conclusion that the e response (rather than the v response) predominantly contributed to the BOLD response remained valid.

Discussion

Here we showed that, independent of the level of adaptation assumed in the neural response, the nonlinearity of the BOLD response to neural activity was similar to that of the estimated

OEF response (Fig. 5). In addition, we showed that the nonlinearity of the [HbT] response as a measure of the blood volume response (Eq. (10)) was consistently less than that of the BOLD and OEF responses (Fig. 5). These results suggested that the nonlinearity of the BOLD response was mainly caused by the nonlinearity of the OEF response, as the BOLD response could be expressed as a function only of the e and v responses (Eqs. (8) and (11)), and the BOLD signal change was four to seven times more influenced by the e response than the v response (Table 2, Fig. 7B).

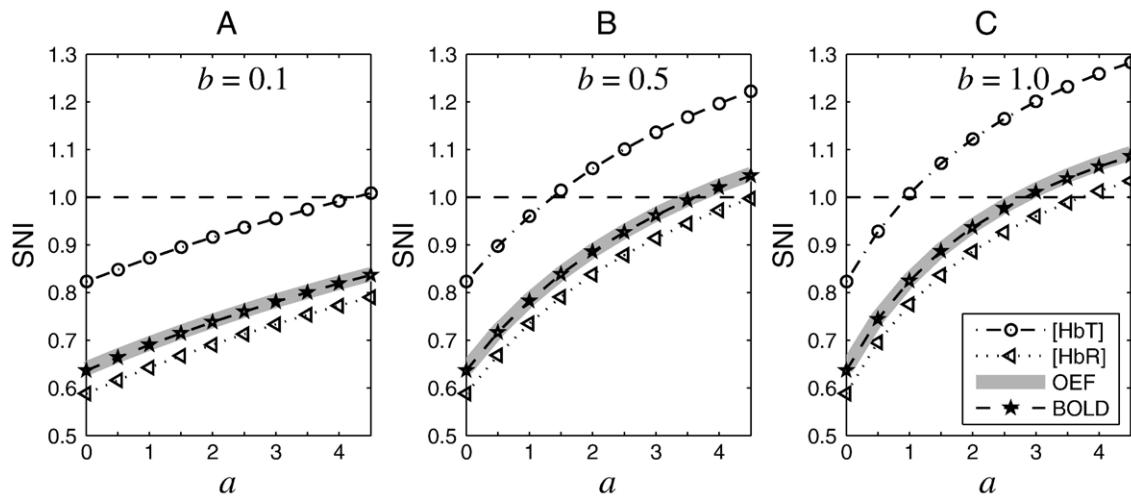


Fig. 5. Plots of the SNI values for the NIRS and fMRI measured as a function of the neural adaptation parameter. The SNI value is plotted against one neural adaptation parameter, a (Eq. (5)), with representative cases of the other neural adaptation parameter, b (A) $b=0.1$, (B) $b=0.5$, and (C) $b=1.0$; Fig. 2). The absolute value of SNI was sensitive to variation in the parameters of the neural adaptation function (a and b), while the relative difference between the SNIs of any two measures was insensitive to these changes. The [HbT] response showed the least saturation nonlinearity. The other responses ([HbR], BOLD, and the estimated OEF) showed relatively stronger saturation nonlinearity.

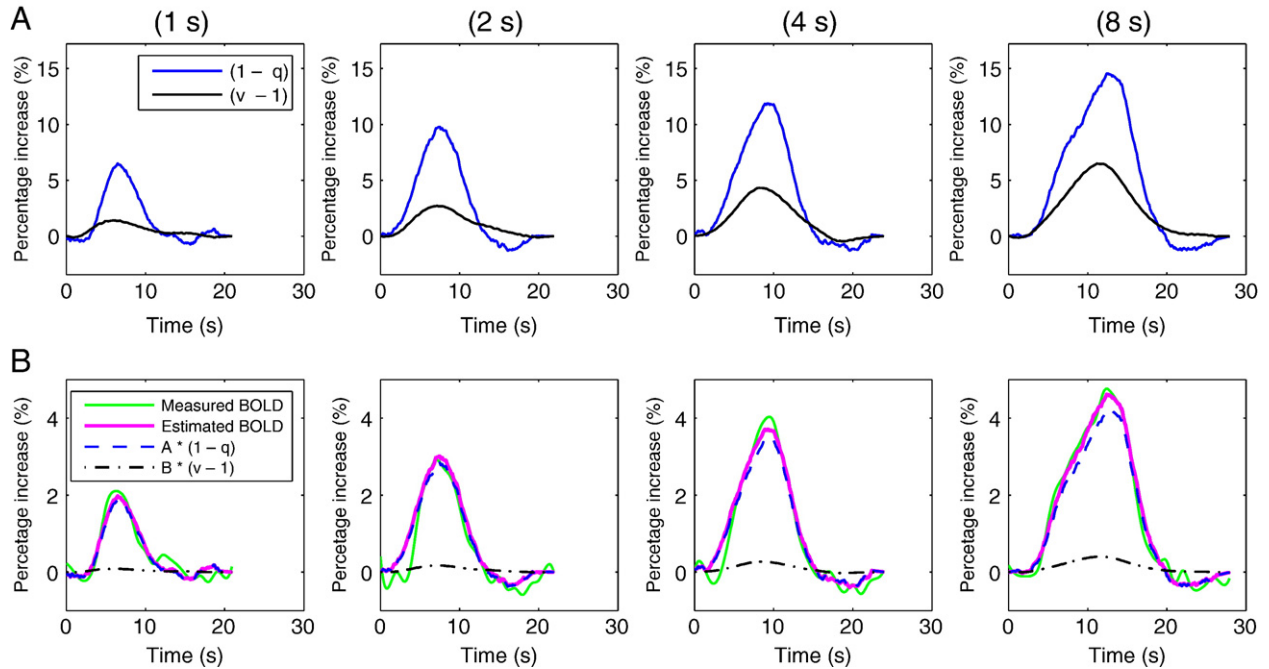


Fig. 6. Results from the model shown in Eq. (8) using our measured fMRI and NIRS time series data. (A) The responses in $(1 - q)$ and $(v - 1)$ are plotted for each stimulus duration. The peak amplitude ratio between the responses decreased with increasing stimulus duration. (B) The $A(1 - q)$ and $B(v - 1)$ responses, as well as the estimated BOLD responses, were superimposed on the measured BOLD responses. The mixture ratio between the q and v responses was estimated to be $A:B=4.68:1$ according to curve fitting, assuming standard baseline parameters (see main text for details). The plots represent the actual contributions of the responses in q and v scaled by A and B , respectively, to the BOLD response. The results indicate that the q response contributed more strongly than the v response. Further results of the fitting test and estimated parameters are shown in Table 2.

Neural adaptations

Various degrees of neural adaptation have been reported in animal and human studies. In the monkey V1 cortex, the adaptation

phenomenon has been observed in the measured response in field potential (Logothetis et al., 2001), while the neural response (field potential) to stimuli has been shown to be linear in the rat somatosensory cortex (Martindale et al., 2005). Thus, different types

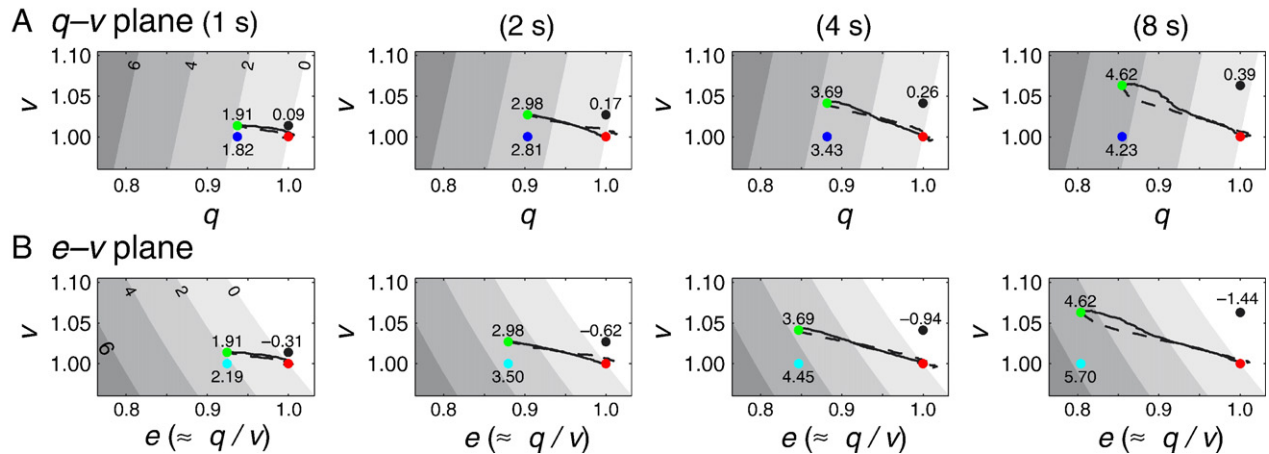


Fig. 7. Trajectory of the BOLD response plotted in the $q-v$ plane (A) and the $e-v$ plane (B), where q , v , and e are the baseline-normalized total [HbR], venous blood volume, and oxygen extraction fraction, respectively (see main text). All of the parameters used in the analysis were the same as those in Fig. 6. The contours are the equivalent BOLD signal lines from 0 to 6% in steps of 2%. The numerical label for each dot represents the percentage increase of the BOLD signal at that point. (A) The slope of the contour in the $q-v$ plane corresponds to the coefficient ratio A/B in Eq. (8). The red dot represents the initial baseline status $(q, v)=(1, 1)$. The green dot denotes the maximum BOLD change $f(q_p, v_p)$. The ascending phase of the response trajectory is shown by the solid line, and the descending phase is shown by the dashed line. The blue dot indicates $f(q_p, 1)$, and the black dot indicates $f(1, v_p)$. (B) The $e-v$ plane is shown using the same format as in panel A. The green dot denotes the maximum BOLD change $g(e_p, v_p)$, the cyan dot indicates $g(e_p, 1)$, and the black dot indicates $g(1, v_p)$. The contours in the $e-v$ plane approximate straight lines within the physiological range of e and v changes. The opposite directions of the contributions of e and v to the BOLD signal change is shown.

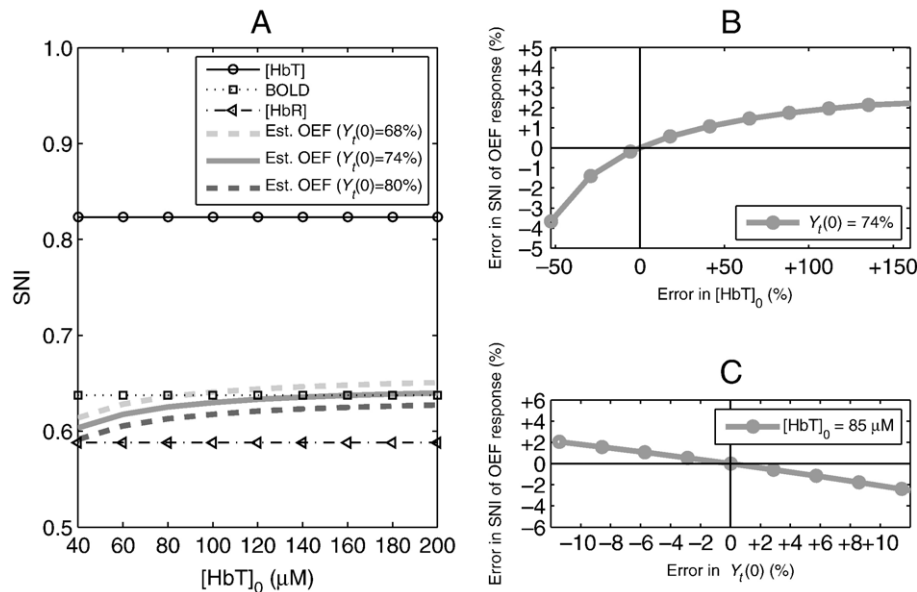


Fig. 8. (A) Plots of the SNI values of the estimated OEF responses as a function of $[HbT]_0$ (ranging from 40 to 200 μM), with varied $Y_t(0)$ values (68, 74, and 80%). The SNI values for the $[HbT]$, $[HbR]$, and BOLD responses are plotted for comparison. The SNI of the estimated OEF response was insensitive to the assumed baseline values for $[HbT]$ and Y_t , when they were varied within physiologically feasible ranges. The percentage error in the estimation of the SNI of the OEF response is plotted against the percentage error from the standard in the assumed variables for $[HbT]_0$ (B) and $Y_t(0)$ (C). The error in the SNI estimates of the OEF response was negligible compared with that associated with the assumptions about the baseline variables. These results represent a case without neural adaptation, but similar patterns were found in the analysis with neural adaptation.

of stimulus might cause different levels of neural adaptation in different cortices. In several human studies (Miller et al., 2001; Soltysik et al., 2004), neural adaptation, which could not be measured directly, was inversely estimated from the BOLD response, with the assumption that the BOLD response to neural activity was linear. These studies also suggested that different stimulus types might cause different levels of neural adaptation in different cortices. However, even for similar visual tasks, the degree of neural adaptation differed between these studies. For example, Miller et al. (2001) reported values for the neural adaptation parameters in Eq. (5) of $a=3$ and $b=0.5$, while Soltysik et al. (2004) gave values of $a=1.5$ and $b=0.6$. These neural adaptation parameters could be estimated uniquely by assuming linearity in the second step. These findings indicate that the degree of neural adaptation might change depending upon the task conditions, even for the same visual task. Therefore, in the present study, based on these reports of the neural adaptation parameters, we manipulated the unknown neural adaptation parameters within a physiologically feasible range, and estimated the neural response from the stimulus pattern in view of neural adaptation.

Two-step model

A two-step model (Fig. 2) was used to estimate the nonlinearity of the MRI-measured BOLD response and the NIRS-measured hemoglobin responses not to stimuli but to neural activity, based on the assumption that the neural response to stimuli (first step) and the BOLD response to neural activity (second step) were independent processes. With the two-step model proposed here, the degree of saturation nonlinearity of the BOLD and hemoglobin responses to neural activity could be estimated as a function of the neural adaptation parameters (Fig. 5). The result showed that the degree of saturation nonlinearity in the second step decreased with increasing

neural adaptation, indicating the complementary relationship in the degree of nonlinearity between the first and second steps. In previous studies (Miller et al., 2001; Soltysik et al., 2004), attempts were made to explain the observed nonlinearity of the BOLD response by neural adaptation alone. Thus, in such cases, by assuming linearity in the second step, the nonlinear component intrinsically assigned to the second step would be estimated improperly as a part of neural adaptation, leading to the overestimation of neural adaptation. On the contrary, our purpose was to investigate the nonlinearity in the second step, without information on neural activity, which cannot be measured directly in human volunteers. Thus, in the present study, the response nonlinearity of the second step was quantified with the neural activity estimated from the stimulus pattern, assuming various neural adaptations.

We showed that the relative degree of saturation nonlinearity of the responses was preserved across the various levels of neural adaptation (Fig. 5). Thus, the two-step model approach enabled us to compare the relative degree of nonlinearity of the BOLD response and the NIRS-measured hemoglobin responses to neural activity, regardless of the degree of neural adaptation. For any degree of neural adaptation assumed in the present study, the relative proximity of the degree of saturation nonlinearity between the BOLD and OEF responses was consistent. The $[HbT]$ response to neural activity showed consistently weaker saturation nonlinearity than that of the BOLD, $[HbR]$, and OEF responses. These relative proximities and differences in the response nonlinearity, which were revealed by the two-step model approach, were sufficient to show the main source of the nonlinearity of the BOLD response.

Assumptions in calculating the $[HbR]$, $[HbT]$, and OEF responses

The estimation of the OEF response from NIRS data was based on assumptions about several parameters, including the path-length

Table 2
Results of the test for the Obata's model with our simultaneously measured fMRI and NIRS data

Stimulus duration (s)	$f(q_p, 1)$ $A(1-q_p)$	$f(1, v_p)$ $B(v_p-1)$	Contribution ratio $f(q_p, 1)/f(1, v_p)$	$g(e_p, 1)$ $A(1-e_p)$	$g(1, v_p) (B-A)$ (v_p-1)	Contribution ratio $g(e_p, 1)/g(1, v_p)$
(i) $Y_v(0) = 0.56$ ($Y_t(0) = 0.67$)						
1	1.82	0.09	21.37	2.29	-0.42	5.51
2	2.81	0.17	16.71	3.70	-0.82	4.51
4	3.43	0.26	13.36	4.74	-1.25	3.79
8	4.23	0.39	10.79	6.14	-1.91	3.21
(ii) $Y_v(0) = 0.65$ ($Y_t(0) = 0.74$)						
1	1.82	0.09	21.37	2.19	-0.31	6.98
2	2.81	0.17	16.71	3.50	-0.62	5.66
4	3.43	0.26	13.36	4.45	-0.94	4.71
8	4.23	0.39	10.79	5.70	-1.44	3.95
(iii) $Y_v(0) = 0.74$ ($Y_t(0) = 0.80$)						
1	1.82	0.09	21.37	2.09	-0.21	9.90
2	2.81	0.17	16.71	3.30	-0.42	7.94
4	3.43	0.26	13.36	4.15	-0.64	6.53
8	4.23	0.39	10.79	5.26	-0.97	5.42

Assuming that the venous blood volume fraction $\gamma(0)=0.75$, and the total blood volume fraction $V_t(0)=0.04$.

factor, the baseline values of the hemoglobin concentration, and the venous blood volume fraction.

The optical path length is required to calculate the regional change in hemoglobin concentration from the change in the NIRS-measured light absorbance. However, we could not measure the path length, which was one of the limitations of our NIRS measurements. The partial path-length factor (PPF) or the DPF is generally used for path-length estimation in NIRS measurements. The PPF is a proportionality factor that converts the source-detector optode distance into the average path length traveled by light through a focal region of chromophore change (Hiraoka et al., 1993; Steinbrink et al., 2001; Uludağ et al., 2002). The PPF depends on the position and volume of the focal-activated brain tissue and the optical properties of the tissue. However, the PPF values are generally unknown and can be temporally altered under specific task conditions. Thus, a reliable PPF value must be directly measured at each channel for each subject and cannot be generalized. For this reason, in the present study, we used the DPF instead of the PPF. This approach generally causes the optical path length to be overestimated, and the $\Delta[\text{HbT}]$ and $\Delta[\text{HbR}]$ to be systematically underestimated, depending upon the factor (PPF/DPF) that indicates the ratio of inclusion of the activated areas in the sampling volume. These errors could be minimized if the sampling volume area was largely activated. However, as current NIRS instruments have relatively low spatial resolution, such errors are generally unavoidable. The effect of the PPF/DPF ratio on the SNI estimation of the OEF response can be approximated using a simulation analysis similar to that shown in Fig. 8. If the PPF/DPF ratio is assumed to be greater than 50%, the error in the SNI of the OEF response should be less than 4%. However, if the ratio is assumed to be 25%, the error in the SNI of the OEF response should be greater than 10%.

In calculating the absolute values of $[\text{HbT}]$ and $[\text{HbR}]$ from $\Delta[\text{HbT}]$ and $\Delta[\text{HbR}]$, we used standard baseline values for these parameters taken from the literature (as described in the Materials and methods section). Assumed values of $[\text{HbT}]_0$ ranging from 75 to 100 μM have been reported (Strangman et al., 2002; Boas et al., 2003). These variations can be regarded as physiologically feasible. When the $[\text{HbT}]_0$ was estimated from the standard blood

hemoglobin concentration (13–15 g/dl) within the blood volume fraction (4%) of the brain tissue, the range of $[\text{HbT}]_0$ values was 81–94 μM . The value of Y_v in the human brain can be monitored by jugular venous oxygen saturation, the reported normal range of which is 55–75% (Shaaban Ali et al., 2001). Assuming the resting venous blood volume fraction (γ_0) was 0.75 (Phelps et al., 1979), the normal range of $Y_t(0)$ values was 66–81% (Eq. (2)). This range was comparable to those reported in previous studies. The normal value for $Y_t(0)$ should also be defined as a range rather than as a fixed point. To investigate the error caused by these assumptions, the results were estimated while varying the assumed baseline values within the physiologically feasible range. According to the simulation (Fig. 8), the assumed values had little influence on the results of the nonlinearity estimates. Hence, these assumptions were not considered as a serious limitation of the present method.

The estimation of the OEF response from the $[\text{HbR}]$ and $[\text{HbT}]$ responses required us to assume a temporally constant value of γ ($\equiv V_v/V_t$). However, γ could change dynamically during the time course of activation. The blood transit time through the capillaries would cause differences in peak time between the V_a and V_v responses. Therefore, as V_t was the weighted sum of V_a and V_v , the peak time of V_v would shift from that of V_t and γ would not be constant. Culver et al. (2003) discussed the error associated with the assumption of a constant γ . However, there is no way to prevent this problem at present, as optical imaging or NIRS cannot measure the V_a and V_v responses separately.

The inflow effect on the OEF response

The balloon model (Buxton et al., 1998; Obata et al., 2004) shows the relationship between the OEF and other physiological parameters under dynamic-state conditions, as follows:

$$\frac{dv}{dt} = \frac{1}{\tau_0} (f_{in} - f_{out}) \quad (13)$$

$$\frac{dq}{dt} = \frac{1}{\tau_0} \left(\frac{E}{E_0} f_{in} - \frac{q}{v} f_{out} \right) \quad (14)$$

Here, f_{in} and f_{out} represent inflow into, and outflow from, the venous compartment, respectively, and τ_0 is the mean transit time. Based on Eqs. (13) and (14), the OEF dynamics can be expressed in a general form according to the following equation (Hoge et al., 2005):

$$\frac{E}{E_0} = \frac{q}{v} + \frac{\tau_0}{f_{in}} \left(\frac{dq}{dt} - \frac{q}{v} \frac{dv}{dt} \right) \quad (15)$$

However, in our study, we used Eq. (4) to approximate the OEF response, as cerebral perfusion was not measured, and thus τ_0 and f_{in} were unknown. The inflow effect on the OEF estimation can be neglected in the block-design paradigm with relatively longer stimulus durations (Hoge et al., 2005). However, when the stimulus duration is brief, it is necessary to consider the temporal derivative term in Eq. (15).

Although, in our case, the E and f_{in} responses cannot be estimated independently, we can assume the following relationship between E and f_{in} :

$$E = 1 - (1 - E_0)^{(1/f_{in})} \quad (16)$$

This was proposed by Buxton et al. (1998). The model is based on the assumption that the flow and oxygen metabolism are tightly coupled. This formula has been used in the simulation of the BOLD response nonlinearity (Friston, 2002). Based on Eq. (16), Eq. (15) can be solved for E , if the remaining unknown parameter τ_0 is assumed to be a constant value. Consequently, we have produced new plots for the OEF response considering the inflow effect (Fig. 9).

When considering the temporal derivative term in Eq. (15) – that is, the inflow effect – the unknown mean transit time (τ_0) had a large influence on the estimation of the OEF response time course: the response waveform was shifted forward in time by approximately τ_0 . When τ_0 was assumed to be 1 s, the response waveform only slightly differed from that when $\tau_0=0$. By contrast, when τ_0 was assumed to be 2 or 3 s, the response waveform changed remarkably compared with that at $\tau_0=0$, suggesting that the temporal derivative term in Eq. (15) should not be negligible in such cases.

The SNI for the OEF response was calculated considering the inflow effect. Despite the remarkable shift in the waveform, the SNI only differed slightly (Table 3). The nonlinearity of the OEF response with respect to stimulus duration was mainly due to the strong nonlinearity of the steady-state term (q/v), although it was reinforced slightly by considering the temporal derivative term (inflow effect) especially when the unknown mean transit time (τ_0) was assumed to be relatively long.

Assumption of constant Hct

To relate the change in [HbT] to the cerebral blood volume, a constant Hct level during activation has been assumed in the optical imaging field (Boas et al., 2003; Culver et al., 2003). In accordance with this convention, we introduced Eq. (10). However, the possibility of changes in Hct during activation has been raised (Kleinschmidt et al., 1996; Jaszewski et al., 2003; Yacoub et al., 2006). Kleinfeld et al. (1998) reported a small but significant decrease in the Hct level after stimulation. Vanzetta et al. (2005) observed that the plasma volume time course was delayed with respect to the [HbT] time course in the cat brain

during and after visual stimulation. The observed difference in the time course between the plasma volume and the [HbT] indicates a change in the Hct level during activation. Both studies reported a decrease in Hct, which reached a minimum slightly after the blood volume level peaked. This could cause the post-stimulus undershoot in the BOLD signal (Jaszewski et al., 2003; Yacoub et al., 2006). This implied that the error due to the non-constant Hct should have appeared in the descent phase of the v response. As the ratio of the coefficients A/B was mainly determined by the amplitude of the major positive (for [HbT]) or negative (for [HbR]) changes of the responses, minor changes in the post-stimulus period of the responses were expected to have little effect on the estimation.

Contributions of q and v to the BOLD response

The contributions of q ($=[\text{HbR}]/[\text{HbR}]_0$) and v ($\approx[\text{HbT}]/[\text{HbT}]_0$) to the BOLD response could be estimated when applying the model of Eq. (8) to our simultaneously measured fMRI and NIRS data (see Materials and methods section). However, in practice, the A/B ratio (Eq. (8)) between the q and v responses could not be obtained easily, as they had similar waveforms (Fig. 6A). Huppert et al. (2006) employed a short-duration event-related motor task to emphasize the subtle temporal differences in the waveforms of the q and v responses, and reported a convincing estimate for the A/B ratio of 4.2. In this case, the resulting A/B ratio might be specific to the stimulus duration of 2 s. In the present study, we measured the BOLD and NIRS responses to stimuli with four different durations. To determine a common A/B ratio, we utilized the differences in the nonlinearity between the [HbR] and [HbT] responses. The ratio of peak amplitude between the q and v responses decreased with increasing stimulus duration, because of the difference in the response nonlinearity between these responses (Fig. 6A). For various stimulus durations, the fractional change in v showed relatively linear responses, while the fractional change in q showed more nonlinear saturated responses. Thus, assuming that A and B were constant across different stimulus durations, we were able to estimate these two parameters robustly. We utilized the standard least squares fitting method implemented via a built-in function of the standard library of Matlab (MathWorks, Sherborn, MA, USA). To confirm the model fitness, we performed a visual inspection of the fitted curves compared with the data, and calculated the residual sums of squares between them. These could help to avoid the problem of a ‘local optimum’. The fitting results could be confirmed by the slight differences between the measured and estimated BOLD response curves. As shown in Fig. 6B, the measured BOLD responses for all the stimulus durations in our experiment were well fitted to those estimated using the model of Eq. (8) with a common A/B ratio. Thus, the present method had the advantage of providing a more general test of the performance of the model of Eq. (8) over a range of stimulus durations rather than for a single-duration stimulus.

Our estimate of the A/B ratio was not consistent with the theoretically predicted value of 2.78 for a TE of 30 ms at 3 T (Mildner et al., 2001; Huppert et al., 2006), although it was basically in agreement with that reported by Huppert et al. (2006). Further studies will be necessary to clarify this discrepancy. However, it might be explained by NIRS-specific errors in our estimation of the A/B ratio, because several assumptions were made in the analysis, including those regarding the baseline values

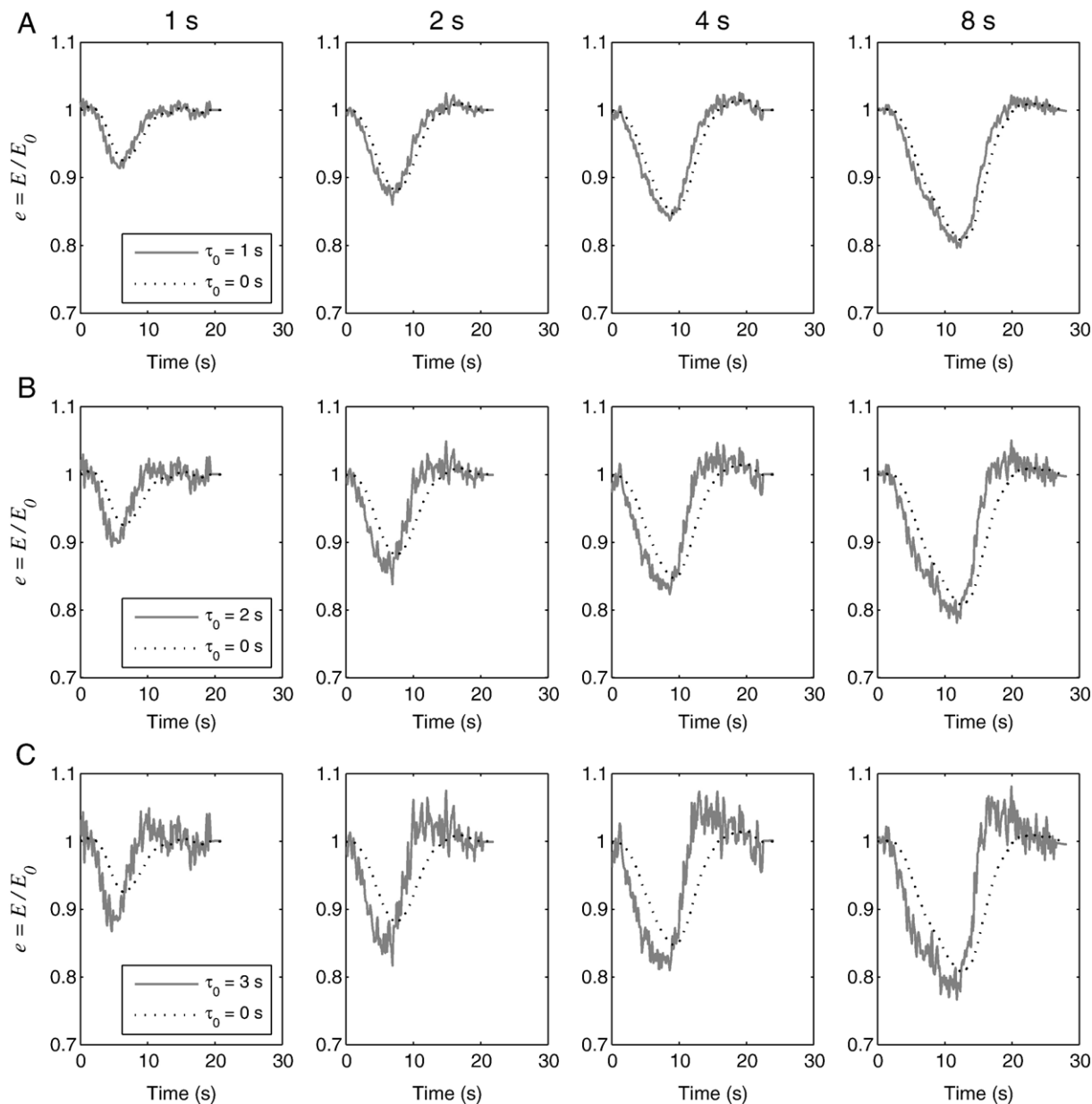


Fig. 9. Plots for the OEF response considering the inflow effect. The estimated time course of $e = E/E_0$ (Eq. (15)) was plotted against time for each stimulus duration with the unknown mean transit time, τ_0 , varied from 1 to 3 s. The plots for the case in which $\tau_0 = 0$, without considering the inflow effect on the OEF estimation, were superimposed onto the same plot. When τ_0 was assumed to be 1 s (A), the response waveform was similar to that for $\tau_0 = 0$. The relatively long τ_0 values of 2 s (B) and 3 s (C), which enhanced the effect of the temporal derivative term in Eq. (15), induced the response waveform to shift forward in time (approximately by τ_0).

of the hemoglobin concentration and the PPF (Huppert et al., 2006).

Contributions of e and v to the BOLD response

We were able to estimate the contributions of e and v to the BOLD response, as well as the contributions of q and v . According to Eq. (8), the BOLD response can be expressed as a function of q and v alone (Eq. (8)). As q can be transformed into the product of e and v (Eq. (11)), the BOLD response can be represented as a function of the e and v responses alone (Eq. (12)).

In contrast to the original model equation (Eq. (8)), the BOLD response cannot be described as the linear sum of the e and v responses. However, in the e - v plane (Fig. 7B), the contribution ratio between e and v to BOLD could be approximately estimated in the same way as the contribution ratio between q and v in the q - v plane (Fig. 7A).

Notably, the slope of the equal-BOLD contour was negative in the e - v plane (Fig. 7B). The $g(e_p, 1)$ was positive and $g(1, v_p)$ was negative, and hence that the directions of the contributions of e and v were opposite. Furthermore, the e and v contribution ratio at the peak BOLD change was calculated to be 4–7:1 (the ratio decreased with increasing stimulus duration). These indicated that the

Table 3
The influence of inflow over the SNI estimation of the OEF response

	<i>a</i>	0	1.5	3
	<i>b</i>	0.5	0.5	0.5
$\tau_0=0$ s		0.63	0.83	0.96
$\tau_0=1$ s		0.63	0.83	0.96
$\tau_0=2$ s		0.62	0.82	0.95
$\tau_0=3$ s		0.61	0.82	0.94

The SNI was calculated for the mean transit times (τ_0) of 0, 1, 2, and 3 s. *a* and *b* represent the parameters characterizing neural adaptation function (Eq. (5)).

decrease in OEF was the major determinant of the BOLD signal increase.

Thus, the contributions of *e* and *v* to the BOLD response, as well as the degree of nonlinearity of the *e* and *v* responses compared with that of the BOLD response, were estimated quantitatively in the present study. From both results, we concluded that the nonlinearity of the OEF response mainly caused the nonlinearity of the BOLD response.

Response nonlinearity estimation and correlation analysis

Hemodynamic response nonlinearity was used to compare the fMRI and NIRS measures quantitatively in the present study. In previous studies in which fMRI and NIRS were measured simultaneously, the correlation coefficient between the time series of the responses has been used for the comparison. However, the NIRS-measured hemoglobin responses showed similar waveforms to each other (Fig. 2), all of which correlated well with the BOLD response. There was a slight difference in the correlation coefficient between these hemoglobin responses, although the [HbR] response was best correlated with the BOLD response. When using longer stimulus durations, the [HbO] response, with a relatively large response amplitude, could be better correlated with the BOLD response than the [HbR] response (Strangman et al., 2002). In this respect, correlation analysis might not be appropriate for differentiating the features of these hemoglobin responses. By contrast, the difference in the nonlinearity of these hemoglobin responses was more prominent than that in the degree of correlation. We found that the [HbT] response, which was not affected by the change in venous blood oxygenation, showed a relatively linear response, whereas the [HbR] response, which was determined from the change in venous blood oxygenation as well as the change in venous blood volume, was highly nonlinear. In addition, we found that the BOLD response showed strong nonlinearity similar to that of the [HbR] response, suggesting that the BOLD and the [HbR] responses share a common physiological mechanism. However, the BOLD response consists not only of the [HbR] response but also of the [HbT] response (Buxton et al., 1998; Obata et al., 2004). The proximity of the nonlinearity of two responses indicates the similarity of the underlying physiological mechanism (that is, the OEF contribution) to them. Thus, in terms of response nonlinearity, the BOLD response was more similar to the [HbR] response than to the [HbT] response and was most similar to the estimated OEF response (Fig. 5). This prompted the speculation that the source of the nonlinearity of the BOLD response was mainly characterized by the nonlinearity of the OEF response.

Significance of the nonlinearity of the OEF response

Estimation of the change in OEF with neuronal activation is potentially important for the issue of flow-metabolic coupling/uncoupling on hemodynamic response, because the OEF represents the ratio between blood flow and oxygen metabolism (corresponding to the oxygen supply and demand of the brain tissue, respectively). NIRS, as well as optical intrinsic imaging, can be used to measure changes in both blood volume and blood oxygenation changes in the tissue. These physiological parameters are major components of the hemodynamic response. In the present study the results from these measures suggested physiological implications of the BOLD response. We showed the nonlinearity of the estimated OEF response, the degree of which was similar to that of the BOLD response. One possible explanation for the nonlinear OEF response is that the increase in oxygen metabolism reaches a plateau in the high blood flow range (Miller et al., 2001). Hence, this nonlinear flow-metabolic coupling phenomenon could be a root cause of the nonlinearity of the BOLD response.

Other nonlinear features of the BOLD response

In the present study, we focused on the major positive component of the BOLD response, the increase of which became saturated with increasing stimulus duration. In addition, other minor components, the so-called initial dip (Menon et al., 1995; Hu et al., 1997) and post-stimulus undershoot (Buxton et al., 1998), might also contribute to the nonlinear character of the BOLD signal change. Although these minor negative components have relatively small amplitude, they cannot be neglected when a short interstimulus interval is used, in which case a successive response might begin before the preceding response has returned to baseline.

These negative changes could also be modeled with NIRS-derived physiological components. To estimate the corresponding minor responses in NIRS measures, the fluctuation in baseline absorbance of NIR lights must be corrected accurately. However, the present technique for baseline correction in measured NIR lights might not be sufficient to detect these minor responses robustly. A more comprehensive approach will be needed in future studies to clarify other nonlinear features of the BOLD response.

Conclusion

Simultaneous fMRI and NIRS in humans allows the non-invasive monitoring of temporal dynamics of the responses of physiological parameters (the OEF and CBV responses estimated from NIRS measures) to stimuli, in relation to the BOLD signal change. The methods presented here allowed us to estimate quantitatively the contribution of the OEF and CBV changes to the BOLD signal change and to compare the level of the nonlinearity of these responses with that of the BOLD response. We found that the BOLD signal increase could be mainly attributed to the OEF decrease, although both OEF and CBV changes were influential components of the BOLD signal change. Independent of the degree of neural adaptation assumed in the estimation of the neural response to stimuli, the nonlinearity of the BOLD response was similar to that of the OEF response and was much greater than that of the CBV response. Therefore, our results support the hypothesis that the nonlinearity of the BOLD response to neural activity is mainly caused by the nonlinearity of the OEF response.

Acknowledgment

This study was supported by a Grant-in Aid for Scientific Research (S#17100003) to N.S. from the Japan Society for the Promotion of Science.

References

- Ardekani, B., Braun, M., Hutton, B., Kanno, I., Iida, H., 1995. A fully automatic multimodality image registration algorithm. *J. Comput. Assist. Tomogr.* 19, 615–623.
- Ardekani, B.A., Guckemus, S., Bachman, A., Hoptman, M.J., Wojtaszek, M., Nierenberg, J., 2005. Quantitative comparison of algorithms for inter-subject registration of 3D volumetric brain MRI scans. *J. Neurosci. Methods* 142, 67–76.
- Birn, R., Saad, Z., Bandettini, P., 2001. Spatial heterogeneity of the nonlinear dynamics in the fMRI BOLD response. *NeuroImage* 14, 817–826.
- Boas, D.A., Strangman, G., Culver, J.P., Hoge, R.D., Jaszewski, G., Poldrack, R.A., Rosen, B.R., Mandeville, J.B., 2003. Can the cerebral metabolic rate of oxygen be estimated with near-infrared spectroscopy. *Phys. Med. Biol.* 48, 2405–2418.
- Boynton, G.M., Engel, S.A., Glover, G.H., Heeger, D.J., 1996. Linear systems analysis of functional magnetic resonance imaging in human V1. *J. Neurosci.* 16, 4207–4221.
- Buxton, R.B., Frank, L.R., 1997. A model for the coupling between cerebral blood flow and oxygen metabolism during neural stimulation. *J. Cereb. Blood Flow Metab.* 17, 64–72.
- Buxton, R.B., Wong, E.C., Frank, L.R., 1998. Dynamics of blood flow and oxygenation changes during brain activation: the balloon model. *Magn. Reson. Med.* 39, 855–864.
- Buxton, R.B., Uludağ, K., Dubowitz, D.J., Liu, T.T., 2004. Modeling the hemodynamic response to brain activation. *NeuroImage* 23 (Suppl 1), 220–233.
- Chance, B., 1991. Optical method. *Annu. Rev. Biophys. Biophys. Chem.* 20, 1–28.
- Cope, M., Delpy, D.T., 1988. System for long-term measurement of cerebral blood and tissue oxygenation on newborn infants by near infra-red transillumination. *Med. Biol. Eng. Comput.* 26, 289–294.
- Culver, J., Durduran, T., Furuya, D., Cheung, C., Greenberg, J., Yodh, A., 2003. Diffuse optical tomography of cerebral blood flow, oxygenation, and metabolism in rat during focal ischemia. *J. Cereb. Blood Flow Metab.* 23, 911–924.
- Duncan, A., Meek, J.H., Clemence, M., Elwell, C.E., Tyszczyk, L., Cope, M., Delpy, D.T., 1995. Optical path-length measurements on adult head, calf and forearm and the head of the newborn infant using phase resolved optical spectroscopy. *Phys. Med. Biol.* 40, 295–304.
- Feng, C.M., Liu, H.L., Fox, P.T., Gao, J.H., 2001. Comparison of the experimental BOLD signal change in event-related fMRI with the balloon model. *NMR Biomed.* 14, 397–401.
- Fox, P., Raichle, M., 1986. Focal physiological uncoupling of cerebral blood flow and oxidative metabolism during somatosensory stimulation in human subjects. *Proc. Natl. Acad. Sci. U. S. A.* 83, 1140–1144.
- Fox, P., Mintun, M., Reiman, E., Raichle, M., 1988. Enhanced detection of focal brain responses using intersubject averaging and change-distribution analysis of subtracted PET images. *J. Cereb. Blood Flow Metab.* 8, 642–653.
- Friston, K.J., 2002. Bayesian estimation of dynamical systems: an application to fMRI. *NeuroImage* 16, 513–530.
- Friston, K.J., Mechelli, A., Turner, R., Price, C.J., 2000. Nonlinear responses in fMRI: the balloon model, volterra kernels, and other hemodynamics. *NeuroImage* 12, 466–477.
- Grubb, R.L., Raichle, M.E., Eichling, J.O., Ter-Pogossian, M.M., 1974. The effects of changes in PaCO₂ on cerebral blood volume, blood flow, and vascular mean transit time. *Stroke* 5, 630–639.
- Hess, A., Stiller, D., Kaulisch, T., Heil, P., Scheich, H., 2000. New insights into the hemodynamic blood oxygenation level-dependent response through combination of functional magnetic resonance imaging and optical recording in gerbil barrel cortex. *J. Neurosci.* 20, 3328–3338.
- Hiraoka, M., Firbank, M., Essenpreis, M., Cope, M., Arridge, S.R., van der Zee, P., Delpy, D.T., 1993. A Monte Carlo investigation of optical pathlength in inhomogeneous tissue and its application to near-infrared spectroscopy. *Phys. Med. Biol.* 38, 1859–1876.
- Hoge, R., Franceschini, M., Covolan, R., Huppert, T., Mandeville, J., Boas, D., 2005. Simultaneous recording of task-induced changes in blood oxygenation, volume, and flow using diffuse optical imaging and arterial spin-labeling MRI. *NeuroImage* 25, 701–707.
- Hu, X., Le, T.H., Uğurbil, K., 1997. Evaluation of the early response in fMRI in individual subjects using short stimulus duration. *Magn. Reson. Med.* 37, 877–884.
- Huppert, T.J., Hoge, R.D., Diamond, S.G., Franceschini, M.A., Boas, D.A., 2006. A temporal comparison of BOLD, ASL, and NIRS hemodynamic responses to motor stimuli in adult humans. *NeuroImage* 29, 368–382.
- Ito, H., Ibaraki, M., Kanno, I., Fukuda, H., Miura, S., 2005. Changes in cerebral blood flow and cerebral oxygen metabolism during neural activation measured by positron emission tomography: comparison with blood oxygenation level-dependent contrast measured by functional magnetic resonance imaging. *J. Cereb. Blood Flow Metab.* 25, 371–377.
- Janz, C., Heinrich, S., Kormmayer, J., Bach, M., Hennig, J., 2001. Coupling of neural activity and BOLD fMRI response: new insights by combination of fMRI and VEP experiments in transition from single events to continuous stimulation. *Magn. Reson. Med.* 46, 482–486.
- Jaszewski, G., Strangman, G., Wagner, J., Kwong, K.K., Poldrack, R.A., Boas, D.A., 2003. Differences in the hemodynamic response to event-related motor and visual paradigms as measured by near-infrared spectroscopy. *NeuroImage* 20, 479–488.
- Kleinfeld, D., Mitra, P.P., Helmchen, F., Denk, W., 1998. Fluctuations and stimulus-induced changes in blood flow observed in individual capillaries in layers 2 through 4 of rat neocortex. *Proc. Natl. Acad. Sci. U. S. A.* 95, 15741–15746.
- Kleinschmidt, A., Obrig, H., Requardt, M., Merboldt, K., Dirnagl, U., Villringer, A., Frahm, J., 1996. Simultaneous recording of cerebral blood oxygenation changes during human brain activation by magnetic resonance imaging and near-infrared spectroscopy. *J. Cereb. Blood Flow Metab.* 16, 817–826.
- Kwong, K., Belliveau, J., Chesler, D., Goldberg, I., Weisskoff, R., Poncelet, B., Kennedy, D., Hoppel, B., Cohen, M., Turner, R., 1992. Dynamic magnetic resonance imaging of human brain activity during primary sensory stimulation. *Proc. Natl. Acad. Sci. U. S. A.* 89, 5675–5679.
- Liu, H.L., Pu, Y., Nickerson, L.D., Liu, Y., Fox, P.T., Gao, J.H., 2000. Comparison of the temporal response in perfusion and BOLD-based event-related functional MRI. *Magn. Reson. Med.* 43, 768–772.
- Logothetis, N.K., Pauls, J., Augath, M., Trinath, T., Oeltermann, A., 2001. Neurophysiological investigation of the basis of the fMRI signal. *Nature* 412, 150–157.
- MacIntosh, B., Klassen, L., Menon, R., 2003. Transient hemodynamics during a breath hold challenge in a two part functional imaging study with simultaneous near-infrared spectroscopy in adult humans. *NeuroImage* 20, 1246–1252.
- Maki, A., Yamashita, Y., Ito, Y., Watanabe, E., Mayanagi, Y., Koizumi, H., 1995. Spatial and temporal analysis of human motor activity using noninvasive NIR topography. *Med. Phys.* 22, 1997–2005.
- Martindale, J., Berwick, J., Martin, C., Kong, Y., Zheng, Y., Mayhew, J., 2005. Long duration stimuli and nonlinearities in the neural-haemodynamic coupling. *J. Cereb. Blood Flow Metab.* 25, 651–661.
- Mehagnoul-Schipper, D., van der Kallen, B., Colier, W., van der Sluijs, M., van Erning, L., Thijssen, H., Oeseburg, B., Hoefnagels, W., Jansen, R., 2002. Simultaneous measurements of cerebral oxygenation changes during brain activation by near-infrared spectroscopy and functional magnetic resonance imaging in healthy young and elderly subjects. *Hum. Brain Mapp.* 16, 14–23.
- Menon, R.S., Ogawa, S., Hu, X., Strupp, J.P., Anderson, P., Uğurbil, K., 1995. BOLD based functional MRI at 4 Tesla includes a capillary bed

- contribution: echo-planar imaging correlates with previous optical imaging using intrinsic signals. *Magn. Reson. Med.* 33, 453–459.
- Mildner, T., Norris, D.G., Schwarzbauer, C., Wiggins, C.J., 2001. A qualitative test of the balloon model for BOLD-based MR signal changes at 3 T. *Magn. Reson. Med.* 46, 891–899.
- Miller, K.L., Luh, W.M., Liu, T.T., Martinez, A., Obata, T., Wong, E.C., Frank, L.R., Buxton, R.B., 2001. Nonlinear temporal dynamics of the cerebral blood flow response. *Hum. Brain Mapp.* 13, 1–12.
- Obata, T., Liu, T.T., Miller, K.L., Luh, W.M., Wong, E.C., Frank, L.R., Buxton, R.B., 2004. Discrepancies between BOLD and flow dynamics in primary and supplementary motor areas: application of the balloon model to the interpretation of BOLD transients. *NeuroImage* 21, 144–153.
- Obrig, H., Israel, H., Kohl-Bareis, M., Uludag, K., Wenzel, R., Müller, B., Arnold, G., Villringer, A., 2002. Habituation of the visually evoked potential and its vascular response: implications for neurovascular coupling in the healthy adult. *NeuroImage* 17, 1–18.
- Ogawa, S., Lee, T., Kay, A., Tank, D., 1990. Brain magnetic resonance imaging with contrast dependent on blood oxygenation. *Proc. Natl. Acad. Sci. U. S. A.* 87, 9868–9872.
- Oja, J.M., Gillen, J.S., Kauppinen, R.A., Kraut, M., van Zijl, P.C., 1999. Determination of oxygen extraction ratios by magnetic resonance imaging. *J. Cereb. Blood Flow Metab.* 19, 1289–1295.
- Pfeuffer, J., McCullough, J.C., Van de Moortele, P.F., Ugurbil, K., Hu, X., 2003. Spatial dependence of the nonlinear BOLD response at short stimulus duration. *NeuroImage* 18, 990–1000.
- Phelps, M.E., Huang, S.C., Hoffman, E.J., Kuhl, D.E., 1979. Validation of tomographic measurement of cerebral blood volume with C-11-labeled carboxyhemoglobin. *J. Nucl. Med.* 20, 328–334.
- Punwani, S., Ordidge, R., Cooper, C., Amess, P., Clemence, M., 1998. MRI measurements of cerebral deoxyhaemoglobin concentration [dHb]-correlation with near infrared spectroscopy (NIRS). *NMR Biomed.* 11, 281–289.
- Rees, G., Howseman, A., Josephs, O., Frith, C.D., Friston, K.J., Frackowiak, R.S., Turner, R., 1997. Characterizing the relationship between BOLD contrast and regional cerebral blood flow measurements by varying the stimulus presentation rate. *NeuroImage* 6, 270–278.
- Robson, M., Dorosz, J., Gore, J., 1998. Measurements of the temporal fMRI response of the human auditory cortex to trains of tones. *NeuroImage* 7, 185–198.
- Shaaban Ali, M., Harmer, M., Latto, I., 2001. Jugular bulb oximetry during cardiac surgery. *Anaesthesia* 56, 24–37.
- Soltysik, D.A., Peck, K.K., White, K.D., Crosson, B., Briggs, R.W., 2004. Comparison of hemodynamic response nonlinearity across primary cortical areas. *NeuroImage* 22, 1117–1127.
- Steinbrink, J., Wabnitz, H., Obrig, H., Villringer, A., Rinneberg, H., 2001. Determining changes in NIR absorption using a layered model of the human head. *Phys. Med. Biol.* 46, 879–896.
- Strangman, G., Culver, J., Thompson, J., Boas, D., 2002. A quantitative comparison of simultaneous BOLD fMRI and NIRS recordings during functional brain activation. *NeuroImage* 17, 719–731.
- Toronov, V., Webb, A., Choi, J., Wolf, M., Michalos, A., Gratton, E., Hueber, D., 2001. Investigation of human brain hemodynamics by simultaneous near-infrared spectroscopy and functional magnetic resonance imaging. *Med. Phys.* 28, 521–527.
- Toronov, V., Walker, S., Gupta, R., Choi, J.H., Gratton, E., Hueber, D., Webb, A., 2003. The roles of changes in deoxyhemoglobin concentration and regional cerebral blood volume in the fMRI BOLD signal. *NeuroImage* 19, 1521–1531.
- Uludağ, K., Kohl, M., Steinbrink, J., Obrig, H., Villringer, A., 2002. Cross talk in the Lambert–Beer calculation for near-infrared wavelengths estimated by Monte Carlo simulations. *J. Biomed. Opt.* 7, 51–59.
- van Zijl, P.C., Eleff, S.M., Ulatowski, J.A., Oja, J.M., Uluğ, A.M., Traystman, R.J., Kauppinen, R.A., 1998. Quantitative assessment of blood flow, blood volume and blood oxygenation effects in functional magnetic resonance imaging. *Nat. Med.* 4, 159–167.
- Vanzetta, I., Hildesheim, R., Grinvald, A., 2005. Compartment-resolved imaging of activity-dependent dynamics of cortical blood volume and oximetry. *J. Neurosci.* 25, 2233–2244.
- Vazquez, A., Noll, D., 1998. Nonlinear aspects of the BOLD response in functional MRI. *NeuroImage* 7, 108–118.
- Villringer, A., Chance, B., 1997. Non-invasive optical spectroscopy and imaging of human brain function. *Trends Neurosci.* 20, 435–442.
- Villringer, A., Planck, J., Hock, C., Schleinkofer, L., Dirnagl, U., 1993. Near infrared spectroscopy (NIRS): a new tool to study hemodynamic changes during activation of brain function in human adults. *Neurosci. Lett.* 154, 101–104.
- Villringer, A., Planck, J., Stodieck, S., B'otzel, K., Schleinkofer, L., Dirnagl, U., 1994. Noninvasive assessment of cerebral hemodynamics and tissue oxygenation during activation of brain cell function in human adults using near infrared spectroscopy. *Adv. Exp. Med. Biol.* 345, 559–565.
- Wobst, P., Wenzel, R., Kohl, M., Obrig, H., Villringer, A., 2001. Linear aspects of changes in deoxygenated hemoglobin concentration and cytochrome oxidase oxidation during brain activation. *NeuroImage* 13, 520–530.
- Yacoub, E., Ugurbil, K., Harel, N., 2006. The spatial dependence of the poststimulus undershoot as revealed by high-resolution BOLD- and CBV-weighted fMRI. *J. Cereb. Blood Flow Metab.* 26, 634–644.